ORIGINAL ARTICLE

Analysis and design optimization of double-sided deep cold rolling process of a Ti-6Al-4V blade

Armin Hadadian[1] · Ramin Sedaghati[1]

Abstract

Deep cold rolling (DCR) is a promising mechanical surface treatment which can be effectively used to improve the fatigue life of components by introducing deep and high beneficial compressive residual stresses on the surface and sub-surface layers. However, the application of conventional DCR on thin-walled geometries such as compressor blades can be very challenging as the applied load can damage the component. Double-sided deep rolling on thin-walled components has been proven to be a viable alternative solution as both sides of the component are treated simultaneously which thus decreases the risk of component distortion. In this study, a high-fidelity non-linear finite element model has been developed to simulate the double-sided DCR process on thin Ti-6Al-4V plate and to predict the residual stress profile introduced by the process and after thermal relaxation due to subsequent exposure to high temperature. The accuracy of the developed finite element model is validated by comparison with the experimental measurement available in the literature. Response surface method (RSM) has then been carried out on results obtained by the high-fidelity FE model to develop predictive analytical models to approximate residual stress profiles induced by the process. The developed analytical models can efficiently replace FE models to perform sensitivity analysis and design optimization of process parameters. Load distribution at high stress areas of a generic compressor blade is considered to formulate a design optimization problem of double-sided DCR process in order to achieve optimal residual stress distributions at room temperature and after thermal relaxation at elevated temperature of 450 °C.

Keywords Deep cold rolling · Multi-objective optimization · Non-linear finite element · Residual stress · Thermal relaxation

1 Introduction

High strength-to-density ratio, high corrosion resistance, and superior biocompatibility are the main advantages of Ti-6Al-4V (Ti64), making it a long been favored titanium alloy for aerospace and biomedical applications. One of the main applications of Ti-6Al-4V in gas turbines is in compressor blades which their lives are mainly limited by fatigue. Therefore, improving the fatigue life to enhance durability and reliability of the blades while maintaining the airfoil shape without undergoing an expensive full-scale redesign is a keen desire of aerospace industry.

A number of mechanical surface treatments including shot-peening (SP), liquid jet peening (LJP), laser shock peening (LSP or simply LP), ultrasonic surface rolling (USRP), low plasticity burnishing (LPB), and deep cold rolling (DCR) have been successfully employed in the past few decades to improve wear resistance, fatigue strength, and corrosion resistance of titanium components by introducing a compressive residual stress in the surface and sub-surface layers [1–3].

Deep rolling (DR), deep cold rolling (DCR), low plasticity burnishing (LPB), ball burnishing (BB), and roller burnishing (RB) are fundamentally similar surface treatment processes where a hydrostatically suspended ball plastically deforms a component surface through mechanical interaction. The main difference is in the tooling design and the way the load is applied or controlled during the process [4]. However, the plastic deformation mechanism in the workpiece under these processes is fundamentally identical.

The substantial advantage of DCR process compared with other mechanical strain hardening methods such as SP, LSP, and LJP is basically its capability to yield an excellent surface

✉ Ramin Sedaghati
ramin.sedaghati@concordia.ca

Armin Hadadian
a_hadad@encs.concordia.ca

[1] Department of Mechanical, Industrial and Aerospace Engineering, Concordia University, Montreal, Quebec H3G 1M8, Canada

finish while producing higher and deeper compressive residual stresses and higher strain hardening [5]. This surface treatment has shown promising applications not only in life extension of brand-new engine parts but also in strengthening and refurbishing of aging aircraft structures, nuclear waste material containers, biomedical implants, and welded joints [6].

There are a number of studies on experimental characterization of the induced residual stresses during DCR processing of Ti-6Al-4V alloys [1, 2, 7, 8]. These have unanimously demonstrated that the DCR process effectively improves the fatigue life of the treated components even at elevated temperatures [2, 8]. LPB has been applied to titanium-, iron-, and nickel-based aero-turbine engine alloys to improve damage tolerance, high-cycle, and low-cycle fatigue performance of blades. The reported studies have shown that the process can improve the damage tolerance of Ti-6Al-4V fan blade in order of magnitude [6, 9]. The level of fatigue life improvement in titanium and nickel-base alloys mainly correlates well with the existence of the maximum residual stress induced in the surface layer where the potential cracking initiates. The induced compressive residual stress can effectively retard fatigue crack initiation in high-cycle fatigue. However, the crack propagation under low-cycle fatigue loading can only be impeded if the compressive residual stress is deep enough in subsurface layers [10].

There are also several experimental studies to establish the correlation between DCR process parameters and the induced residual stress profile and the surface finish of the treated components using Design of Experiment (DoE) techniques [11–15]. The investigations have confirmed that DCR is a complex process and each parameter has a different level of interactions on the final state of the surface roughness and induced residual stress profile. Due to cost associated with experimental studies, it is not possible to explore large design space and systematically explore the effect of tool and process parameters simultaneously.

The residual stress generated in the workpiece during the DCR process is the resultant of a complex cyclic plastic deformation and microstructural textural evolution occurred on the surface layer. The process is a highly non-linear dynamic phenomenon because of the dynamic motion of the ball, presence of plasticity beneath the rolling ball, and non-linear contact between the rolling ball and the component [4].

Although the closed form (analytical) solutions with a certain level of accuracy exist for elastic rolling contact, application of semi-analytical methods and finite element (FE) methods are inevitable for the elastic-plastic rolling contact problems. The apparent shortcoming of semi-analytical methods are the inherited inaccuracies in solving large plastic deformation especially under highly non-linear contact conditions and their limitations to two-dimensional rolling contact problems [13].

The determination of optimal process parameters through experiments requires cost-extensive measurements and time-consuming experimental set-ups. On the other hand, the accuracy of the analytical model is inadequate because of the nonlinearities associated with the material plasticity and contact between the ball and workpiece. Finite element (FE) analysis has been proposed as an effective and cost-reducing alternative to experimental and analytical methods [16–18].

Lim et al. [19] simulated DCR process on Ti-6Al-4V plate using a 3D FE model in order to investigate the residual stress distribution at the boundary between the treated and untreated zones on the surface of the component. The results of the FE model in the treated zone were compared with experimental measurements which showed disagreement particularly at the near-to-surface depth. The limitation of the residual stress measurement method at the surface layer area was stated as a potential source of the discrepancy. Klocke et al. [17] had successfully developed a 3D FE model to simulate the deep rolling process on several geometries representing typical features of turbine blade and turbine disk components. Ti-6Al-4V and IN718, the two widely used materials in aerospace industry, were considered in their study. Their study clearly demonstrated that the residual stress distributions in plane geometry and thin-walled geometries are significantly different. While the process affects plane geometry only in the neighborhood of the processed surface, thin-walled geometries are influenced over their entire thickness.

Klocke et al. [5] also investigated the effect of the component thickness on the residual stress distribution induced by deep rolling on IN718 specimens with different thicknesses. The experimental results showed that the thickness of the treated component can significantly influence the near-surface residual stresses. Therefore, the process parameters should be selected based on the component thickness particularly for thin-walled geometries where the thickness of the component is comparable to the residual stress depth. Otherwise, the process may create a detrimental tensile residual stress which can negatively impact the component's fatigue strength.

DCR process tends to create a compressive residual stress on the surface layer which is balanced by tensile residual stress in the inner sub-surface region of the component as the residual stresses in the specimen must be in equilibrium. A component with a thickness larger in order of magnitude than the depth of residual stress is only locally affected in the surface layer while a thin-walled geometry with a thickness comparable to the depth of the residual stress is affected over the entire thickness. This results in a significantly different residual distribution through the thickness in thin-walled components compared with that in thick components [20].

Avoiding permanent deflection under the unidirectional rolling loads is the biggest challenge in DCR process of thin-walled components such as fan and compressor blades

[20]. In addition, the induced strain state in conventional roller burnishing is asymmetrical as the component is treated only on one side. This permanent deflection of the blade is accompanied with increase of the plastic strain in the surface layer which can distort the treated component [20]. Considering this, performing the conventional DCR on thin-walled geometries is not generally recommended and deep rolling of turbine blade is a challenging process [21].

ECOROLL Corporation Tool Technology [22] has designed a special tool to perform double-sided DCR process on thin-walled components such as turbine blades which is shown in Fig. 1. This tool compromises a double-sided hydrostatic deep rolling tool which pressures the balls on both sides of the component simultaneously to avoid the component distortion under the process.

Another risk associated with conventional DCR process of thin-walled component is thermal distortion caused by relaxation of asymmetrical residual stresses induced by the process at room temperature. The distortion can be more severe in component with a comparable thickness to the depth of the plastically deformed zone particularly under a non-uniform thermal distribution [10]. On the other hand, the double-sided process introduces a symmetrical residual stress and plastic deformation through the component thickness which can also mitigate the thermal distortion risk.

Most of the deep-rolled components are intended to operate at elevated temperature where the induced residual stresses are relaxed and redistributed [2, 7]. While there are several studies addressing FE simulation of the DCR process to predict the induced residual stresses at room temperature, very limited studies have addressed the thermal relaxation of induced residual stresses at the elevated temperature.

Prevéy et al. [10] developed a FE model to study permanent deformation of a blade geometry due to thermal relaxation of residual stresses induced by shot peening. The residual stress fields were impor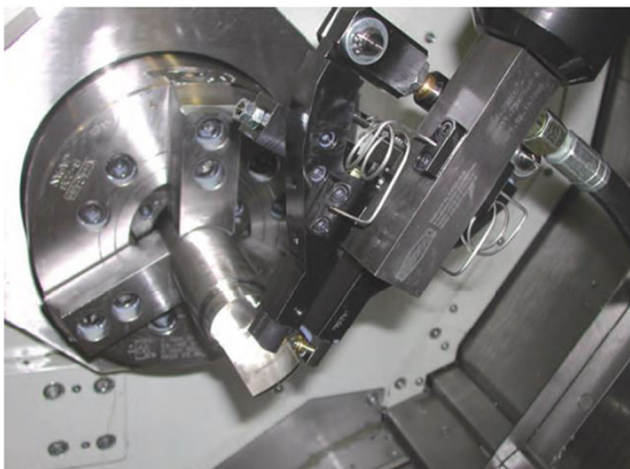ted as an initial state input and then the thermal relaxation was simulated. The results showed that the blade deformation was significantly lower for a uniform relaxation on both sides compared with non-uniform relaxation.

Hadadian and Sedaghati [4] developed non-linear 3D finite element models to simulate the DCR process on Ti-6Al-4V specimens and the following short-term exposure of the treated components to an elevated temperature of 450 °C. The models were able to predict the residual stresses induced by the process and the relaxation due to exposure to the elevated temperature. The finite element predictions correlated well with experimental results with errors generally less than 10%.

As it was discussed earlier, application of double-sided DCR can mitigate the main risks of damaging thin components during conventional DCR and thermal distortion caused by asymmetry relaxation of the residual stresses. However, the process parameter selection for double-sided DCR process is more challenging and crucial for thin-walled components as during the process, the induced residual stresses on each side of the specimen affect the entire thickness and substantially interact and influence the process applied on the other side. The resultant strain hardening may lead to tensile residual stress on surface which can negatively impact the fatigue life of the treated component.

The main contributions of the present study are: (1) Development of a high-fidelity finite element (FE) model to accurately simulate the double-sided deep cold rolling process on thin Ti-6Al-4V plate at room and after exposure to high temperature and (2) Development of an optimization formulation using approximate surrogate models to identify the optimal process parameters. FE models are first developed to simulate double-sided DCR process on Ti-6Al-4v plate with 1 mm thickness. The accuracy of the developed FE model to predict residual stresses is then validated by comparison with the experimental measurements available in the literature [17]. The thermal relaxation of the residual stresses in the following short-term exposure of the treated components to elevated temperature 450 °C is then studied using the developed FE model.

The response surface method has then been carried out on the results obtained from the high-fidelity FE model to develop predictive analytical models to approximate residual stress profiles with respect to the process parameters (i.e., ball diameter, feed, and rolling pressure). The developed analytical functions are considerably lower in order than a full-scale finite element simulation and thus can efficiently replace FE models to perform sensitivity analysis and design optimization of process parameters. A design optimization problem is formulated considering the stress distribution in highly stressed locations of a generic compressor blade, in order to identify optimal parameters of double-sided DCR process to achieve residual stress distributions effective to enhance the fatigue life at room temperature and after thermal relaxation at an elevated temperature of 450 °C.

Fig. 1 Double-sided deep rolling of a turbine blade [22]

2 Finite element simulation

It was discussed earlier that the prediction of the residual stresses introduced by DCR process requires FE simulation because of high level of non-linearity associated with rolling dynamic, friction contact, and plasticity behavior of the material. The level of non-linearity is even higher on the double-sided DCR process of thin-walled geometries as both sides of the component are treated simultaneously and the induced plastic deformation from one side interacts with the plastic deformation of the other side and as a result impacts the introduced residual stresses.

ABAQUS software has been used in the present study to develop the non-linear 3D FE models to simulate the double-sided DCR process on a thin Ti-6Al-4V plate with a 1-mm thickness, and then the subsequent short-time thermal exposure to 450 °C. The predicted residual stress profile after spring back analysis using the developed FE model has been compared with experimental measurement reported by Klocke et al. [17] for the purpose of validation. The thermal relaxation analysis has been subsequently conducted using a validated finite element methodology [4].

The FE model to simulate the DCR process has been developed in the ABAQUS/Explicit environment as it can handle the high non-linearities due to friction contact, plastic deformation, and dynamic loading efficiently and accurately. However, the spring back and thermal relaxation analysis steps are quasi-static in nature and thus have been modeled in ABAQUS/Standard environment which employs implicit integration methodology. Figure 2 presents the sequence of simulations undertaken to model the DCR process and the following thermal loading in order to calculate the induced residual stress and its subsequent relaxation during thermal exposure.

Since the double-sided DCR process, which is schematically demonstrated in Fig. 3(a), is symmetrical with respect to X-Z plane, only half of the workpiece is modeled and the YSYMM symmetry boundary condition in ABAQUS is applied on the midface (symmetry plane). The process induces residual stresses with high gradient in the neighborhood of contact region which demands a very fine mesh to obtain an accurate stress prediction. Therefore, the surface layer beneath the contact zone has been discretized with a very fine mesh with the size of 25 μm. Since the model benefits from the defined symmetry BC to reduce the computational cost, it was possible to mesh the whole geometry uniformly using 640,000 C3D8RT elements in ABAQUS environment as presented in Fig. 3(b). This element is an eight-node thermally coupled brick element accommodating temperature degree of freedom (DOF) in addition to translational displacement DOFs.

The DCR process can be applied under either force control or displacement control of the rolling ball. While the force control mode ensures that a constant load (pressure) is applied to the ball during the process, under displacement control mode, the process is performed under a defined displacement which is prescribed at the end of ball indentation step. The reference experimental study reported by Klocke et al. [17] was conducted under load control which has been also considered in this study.

The DCR process is modeled in a series of simulation steps until a stable residual stress field is achieved in the contact
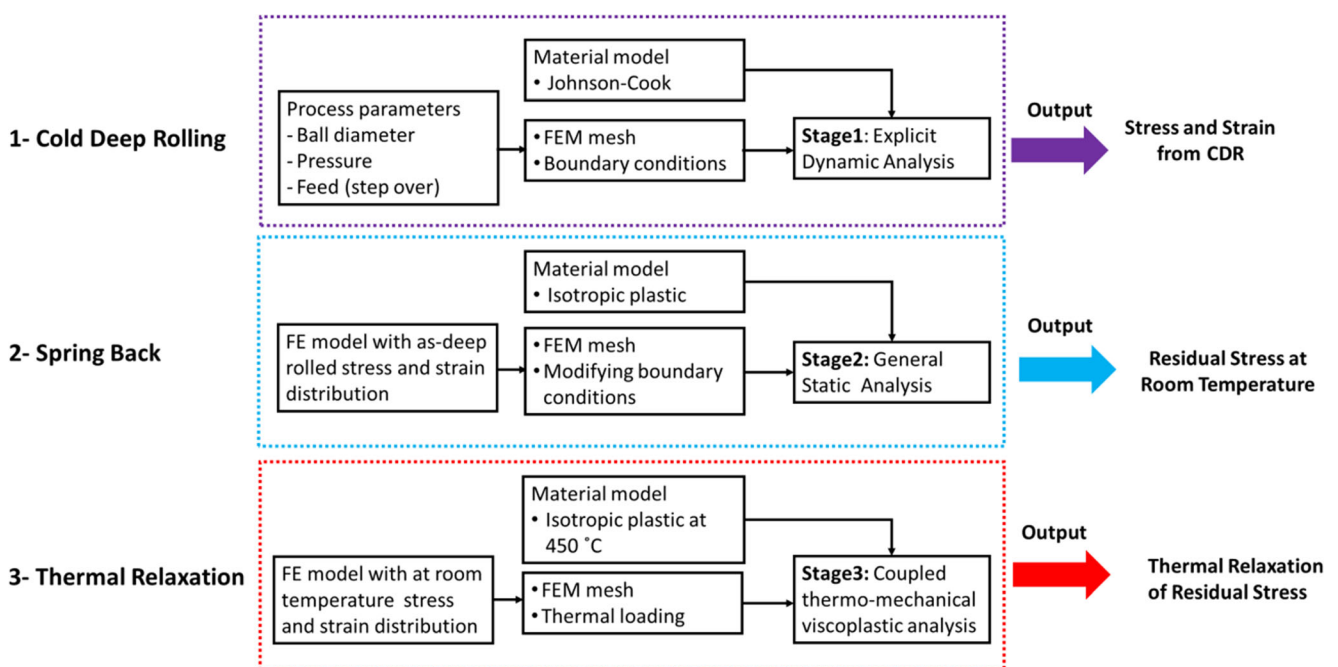

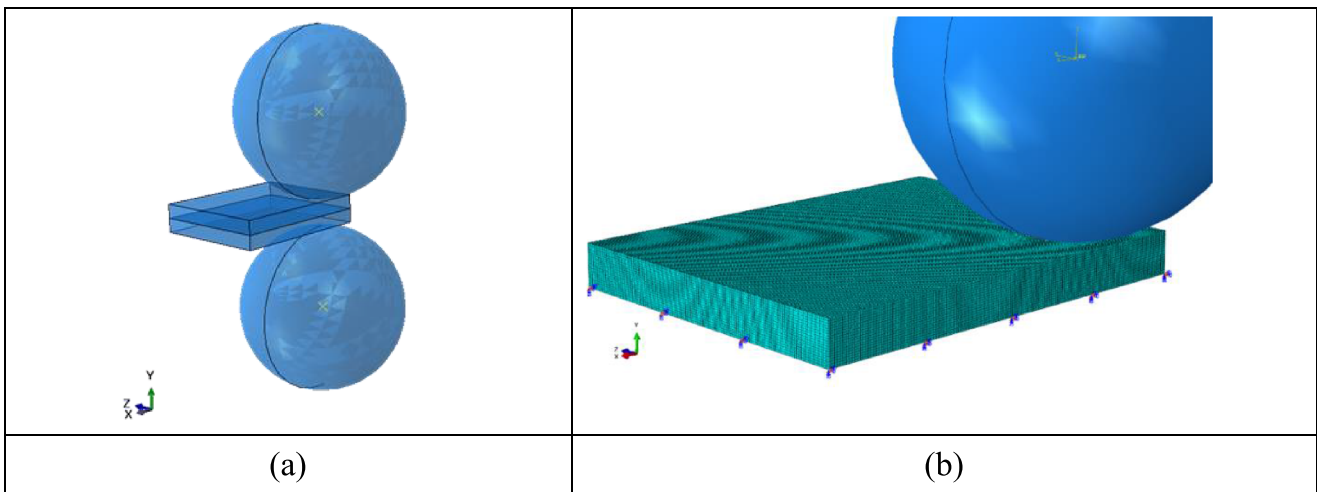Fig. 2 Flow chart for the CDR and thermal relaxation simulations

Fig. 3 **a** Geometric model and **b** FE BC and mesh of the workpiece in the 3D simulation

zone. The roller is assumed to be rigid and its kinematics is defined in four steps by related boundary conditions [4], namely indentation, rolling, feed, and retraction steps. In the indentation step, a constant force is applied to the rigid ball to create a small indentation on the surface of the specimen in − Y axis. The ball is then allowed to roll freely in the + X direction to complete a pass while the applied force is kept constant. This is followed by moving the ball in lateral direction (+ Z) perpendicular to the rolling pass in the amount of feed and then again rolling the pressurized ball but now in − X direction. Based on the amount of feed, overlap would exist between successive rolling passes. Finally, the ball is retracted from the surface in the retraction step.

It has been reported that the effect of friction coefficient on the simulation is negligible as long as the friction is non-zero as any level of friction will allow the ball to be in a pure rotating state of motion [19]. Isotropic Coulomb friction model with friction coefficient of 5×10^{-3} has been considered in this study to model the interaction between the workpiece and ball.

Johnson-Cook (JC) material model has been successfully utilized to describe the material behavior in the simulation of cold rolling processes of Ti-6Al-4V [4]. This material model is purely empirical and describes the flow stress as the function of strain, temperature, and strain rate. The capability of JC model to describe the plastic deformation of Ti-6Al-4V has been demonstrated in several studies [23–25]. The model can be described as:

$$\sigma = [A + B\varepsilon^n]\left[1 + Cln\overset{*}{\varepsilon}\right]\left[1-\left(\frac{T-298}{T_m-298}\right)^m\right] \quad (1)$$

where σ and ε are the effective stress and strain, respectively; $\overset{*}{\varepsilon}$ is the normalized effective plastic strain rate; n is the work hardening exponent; and A, B, C, and m are constants which are determined from an empirical fit of flow stress data. T_m

represents the melting temperature. The material's constants (A, B, C, and m) depend on the range of stress and temperatures considered in the material testing procedure. Therefore, they are not fixed and change under different material testing conditions [23–25].

The JC model developed by Lee and Lin [26] has been considered for FE simulation of DCR of Ti-6Al-4V based on the typical strain range and strain rate expected in DCR process [4]. Since the previous FE results were correlated very well to the experimental measurements, the same JC material model which is presented in Table 1 has been considered in the current study.

The residual stress state changes by preforming each rolling pass until it reaches a saturation in a stabilized region where further rolling the workpiece will not alter the residual stress. It has been previously shown that ten rolling passes, which covers a part of the surface, are sufficient to develop a stabilized region to extract the results while saving the numerical computation time [4].

The residual stress and strain fields evaluated at the end of the DCR process are then imported as initial conditions to the spring back analysis which is modeled using isotropic plasticity behavior of the material at a low strain rate. Twelve vertical lines normal to the treated surface and through the component thickness have been considered in the stabilized region to extract the FE results and calculating the average value at each depth (y-coordinate from the top surface).

The relaxation and redistribution of the residual stresses during the following short-term thermal exposure to 450 °C

Table 1 JC material constant parameters presented for Ti-6Al-4V [26]

A (MPa)	B (MPa)	N	C	m
724.7	683.1	0.47	0.035	1

are then modeled through the plastic softening mechanism where the outcome of the spring back analysis is considered as the initial state input for the analysis. Since the thermal relaxation is quasi-static, the plastic material model at lower strain rate is required for the analysis. Temperature dependent quasi-static stress-strain curves at the strain rate of $1 \ sec^{-1}$ presented by Haight et al. [27] had been successfully adapted in the form of isotropic plasticity to simulate the thermal relaxation of DCR-induced residual stresses in Ti-6Al-4V [4].

The double-sided DCR process treats both sides of the component simultaneously which results in a different material flow and plastic hardening and deformation compared with conventional DCR process. In this study, both processes have been simulated on a plate with a 1-mm thickness under load control mode with process parameters of ball diameter 9 mm, feed 0.200 mm, and rolling pressure 20 MPa. The results for tangential residual stress (z-direction) through the thickness are presented in Fig. 4.

As it can be realized, the residual stress profile induced by double-sided DCR process is significantly different than that induced by the conventional DCR process performed on the same workpiece under identical processing parameters. Under simultaneous deep-rolling process of the two sides of a thin-walled component, the strain hardening induced from one side is deep enough to interact with the rolling process on the opposite side which consequently lowers the plastic deformation imposed on the opposite side and also the induced residual stress through the affected zone. However, as it can be seen, the double-side CDR creates compressive residual stress on both sides of the component which can be important for fatigue enhancement under some applications.

As it can be realized, the thermally relaxed residual stresses at an elevated temperature of 450 °C are also more uniform for double-sided CDR compared with the conventional one

which can mitigate the thermal distortion due to relaxation of asymmetrical residual stresses.

2.1 Validation of the developed FE model

The FE results of double-sided DCR process developed in the current study have been compared with simulation and experimental results reported by Klocke et al. [17], where double-sided DCR treatment of a 1-mm thick Ti-6Al-4V plate was performed using a ball diameter of 6 mm, rolling pressure of 150 bar, rolling velocity of 10 mm/s, and coverage of 60%. Since the amount of the lateral movement of the rolling ball in Z-direction (feed) was not explicitly provided in the reference [17], the simulation was first run only for one rolling pass to obtain the track width and then the feed was determined using the given coverage. The DCR process was then continued considering the calculated feed of 0.240 mm for the next nine subsequent rolling passes until a stabilized region is achieved.

Residual stresses are the result of inhomogeneous plastic deformation generated in component during DCR process. The final state of the material flow defines the direction of reaction forces by the surrounding materials which subsequently describes the nature (compressive or tensile) of the introduced residual stresses. In other words, under a certain rolling force with a given ball dimeter, the sign of the residual stresses in axial and tangential directions can alter depending on the material flow caused by the different amounts of feed.

It has been demonstrated that the residual stress distribution can be explained by the net material flow and the resulting plastic strain [19]. The plastic deformation mechanism during the DCR process is the resultant of the material displacements in the treated zone attributed to three simultaneous deformation mechanisms, namely as the ball rolling (in x direction), the lateral movement of the ball (the feed in z direction), and
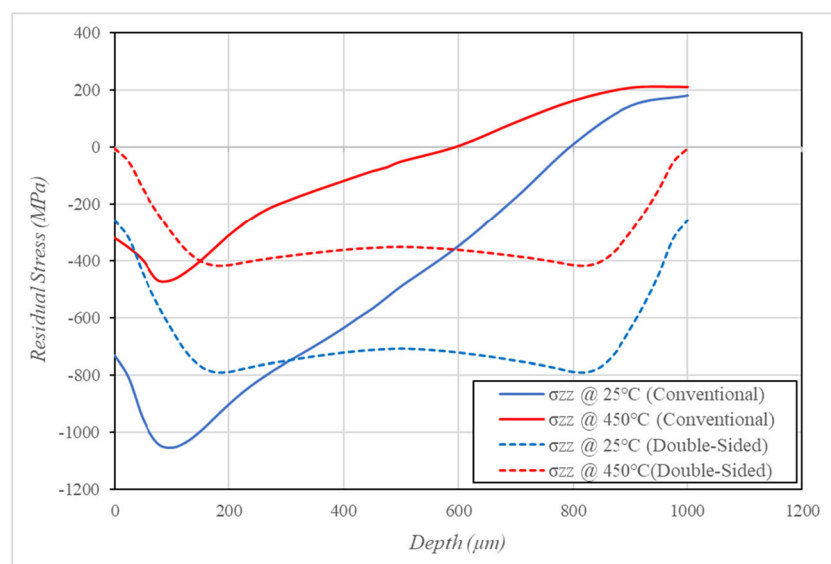

Fig. 4 Residual stress profile in tangential direction at 25 °C and 450 °C obtained by conventional versus double-sided DCR

the vertical movement of the ball (under the rolling force in y direction) which interact with each other during the whole process.

The equivalent stress beneath the ball reaches the yield stress of the workpiece material under a substantial rolling force which results in plastic deformation. A detailed stress analysis of the process reveals a large area of vertical compressive stress directly beneath the rolling ball causing a vertical plastic compression, which leads to plastic extension in the surface of the workpiece. Because of the constant volume of the material, the extension of the surface of the material in one direction leads to a traverse contraction of the material in the perpendicular directions on the surface as well as in the material beneath the surface layer. This results in lateral displacement of the material surrounding the contact zone and consequently developing residual stresses as a reaction to this plastic material displacements.

Figures 5 and 6 respectively show the material flows and plastic deformation in the stabilized region for the process parameters of $D = 6$ mm, $f = 0.240$ mm, and $P = 15$ MPa using the developed FE model. It is noted that to reduce the computational cost, the simulation was conducted only on half of the thickness due to the symmetry about the X-Z plane. The deflection scale has been set to six and the component has been sectioned using the cutting plane for the sake of better visualization.

Figures 7 and 8 respectively show the residual stresses in axial and tangential directions in the stabilized region at both room temperature and 450 °C predicted by the developed FE model. As it can be realized, the process

introduces anisotropic residual stress fields which are significantly different in the axial and tangential directions. The thermal relaxation causes material softening and the subsequent material flow and plastic deformation redistribute the residual stresses. Developing residual stresses in the treated area results in a compensatory residual stress in the surrounding material which plays an important role in the final state of the residual stress field in the treated area after thermal relaxation.

The tangential residual stress values (σ_{zz}) through the depth of the components were extracted along 12 lines in the Y-direction spread over the stabilized region and the average values were calculated and compared with the experimental measurements. Figure 9 shows the results of the tangential residual stress through the thickness predicted using the developed FE model in the present study and comparison with those of experimental measurements and the simulation results reported by Klocke et al. [17]. As it can be seen, the developed FE model can predict the residual stress profile more accurately than the FE model previously developed by Klocke et al. [17].

Compared with the current simulation results, experimental results mainly underpredict the residual stress. It should be noted that the residual stress measurement involves material removals which cause inevitable relaxation and redistribution of the initial residual stress profile. The equilibrium of forces between the tensile region and compressive region must maintain after each step of layer removal resulting in reduction or even elimination of the compressive stress region [28]. The relaxation can be

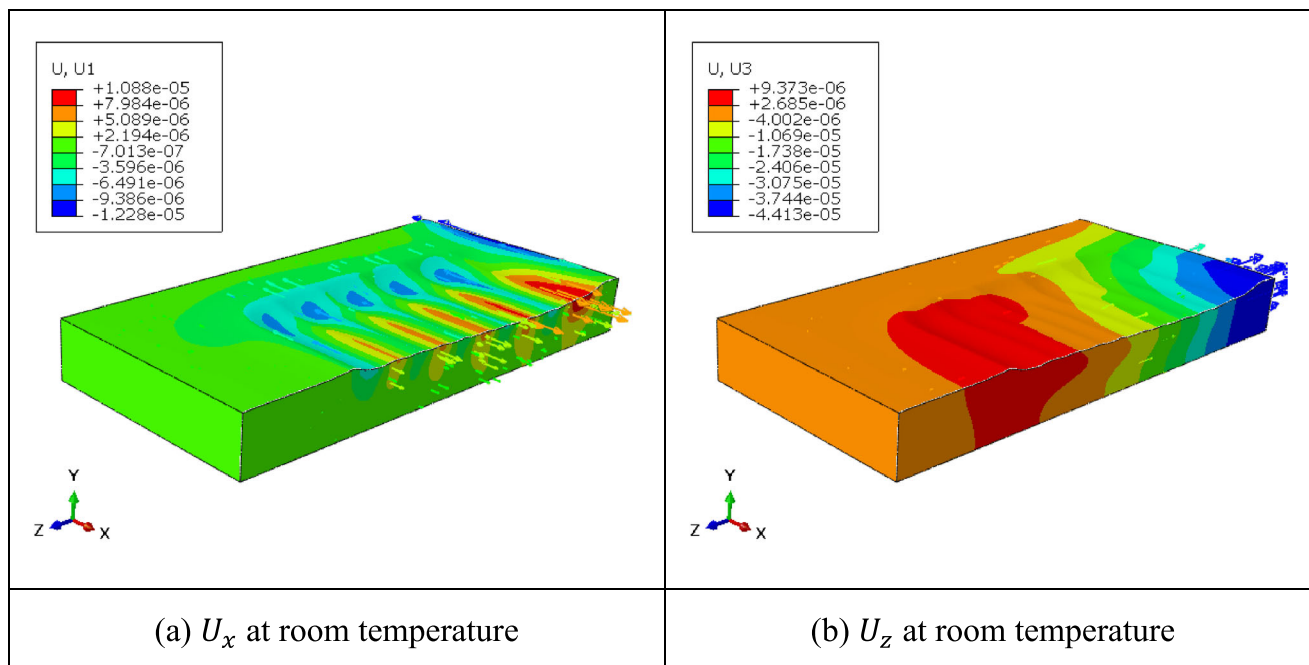(a) U_x at room temperature

(b) U_z at room temperature

Fig. 5 Material displacement after spring back at room temperature in the stabilized region **a** in axial direction and **b** in tangential direction, under force control DCR
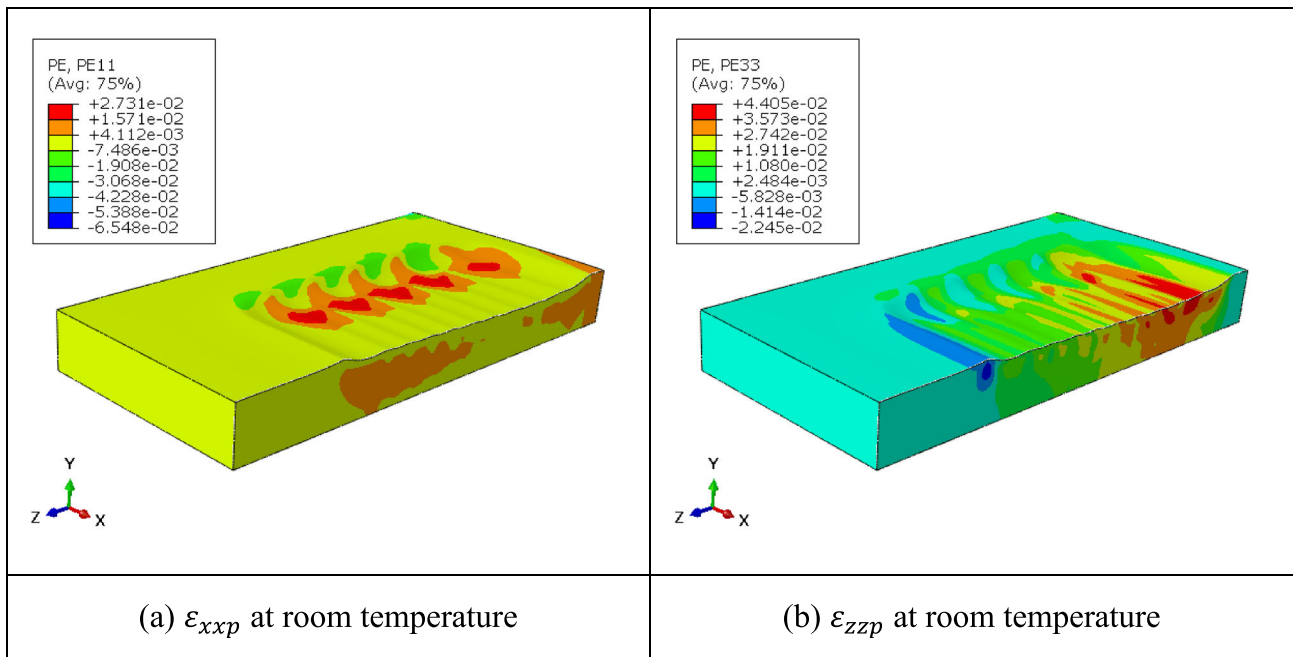
| (a) ε_{xxp} at room temperature | (b) ε_{zzp} at room temperature |

Fig. 6 Plastic strain after spring back at room temperature in the stabilized region **a** in axial direction (ε_{xxp}) and **b** in tangential direction (ε_{zzp}), under force control DCR

greater for thin-walled specimen as the volume of the treated region is less compared with thick components. The inevitable stress relaxation caused by the material removal in electropolishing was not considered in the measurements reported by Klocke et al. [17] which may result in slight underprediction of the residual stress beneath the surface. Considering the measurement errors and assumptions involved in the FE simulation including the assumed material model and ignoring the impact of initial surface roughness and residual stress of the component prior to the deep rolling, the results of the FE models developed in the current study are generally in a very
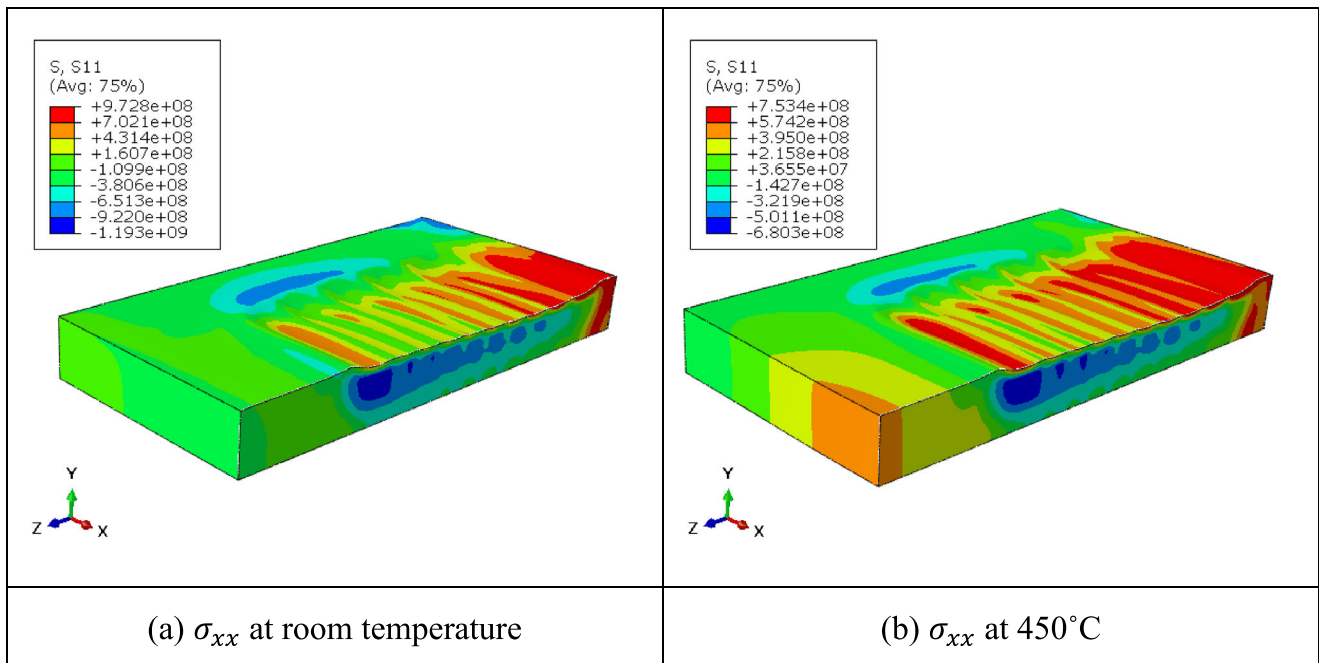

| (a) σ_{xx} at room temperature | (b) σ_{xx} at 450˚C |

Fig. 7 Residual stress (Pa) in axial direction (σ_{xx}) sectioned in the stabilized region **a** after spring back at room temperature and **b** after thermal relaxation at 450 °C under force control DCR

| (a) σ_{zz} at room temperature | (b) σ_{zz} at 450˚C |

Fig. 8 Residual stress (Pa) in tangential direction (σ_{zz}) sectioned in the stabilized region **a** after spring back at room temperature and **b** after thermal relaxation at 450 °C under force control DCR
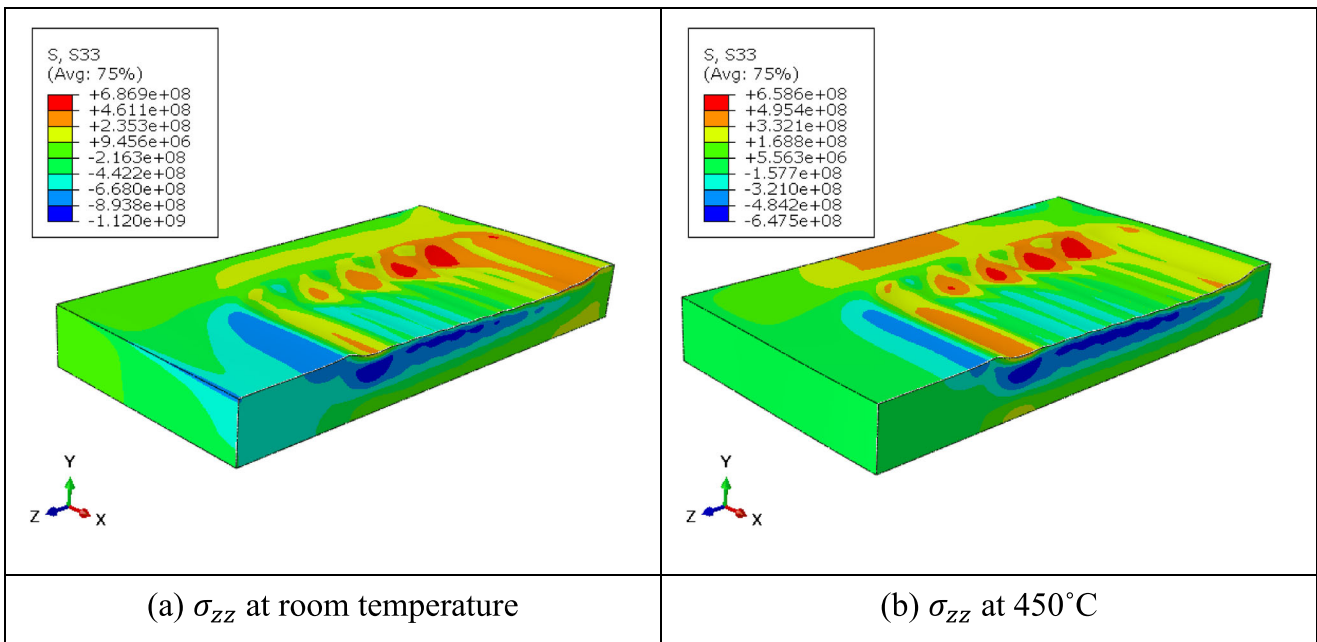
good agreement with the experimental measurements and thus the model can be confidently utilized to simulate the double-sided DCR process.

Figure 10 shows induced residual stress distributions in axial (σ_{xx}) and tangential (σ_{zz}) directions through half the thickness at both room temperature and 450 °C. As it can be realized, the double-sided DCR process generates significantly different residual stress distributions in axial and tangential directions at room temperature and the subsequent exposure to elevated temperature causes relaxation and redistribution of
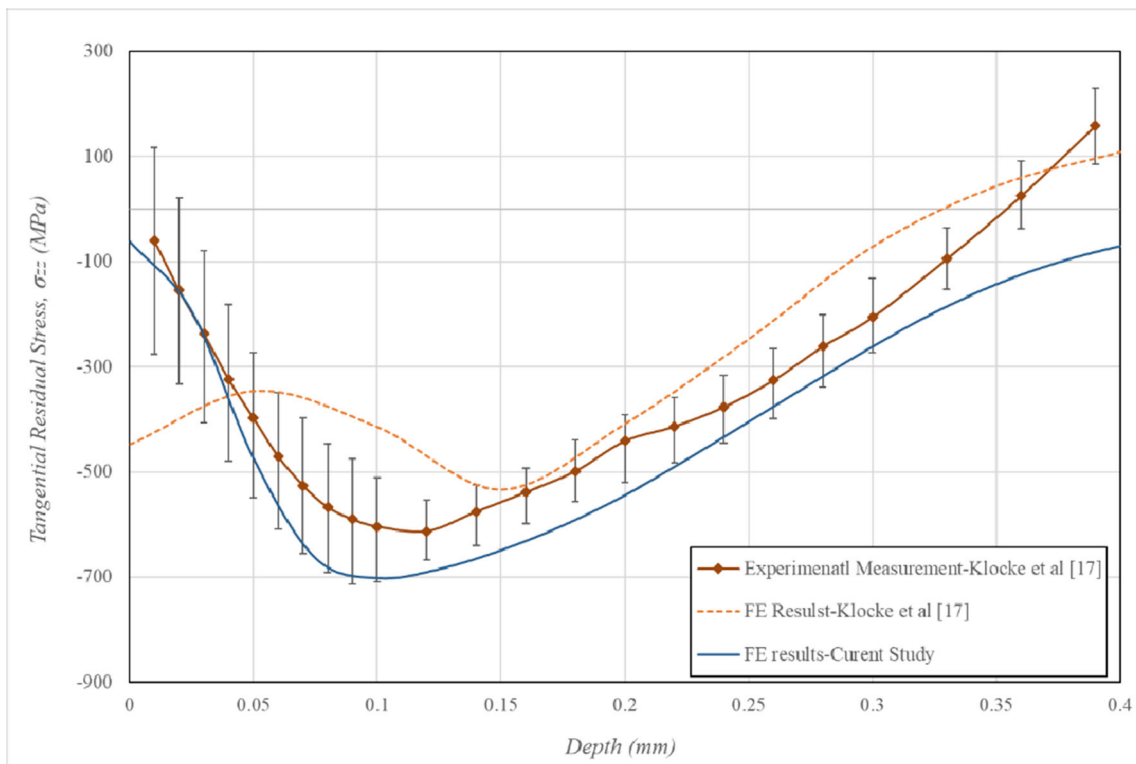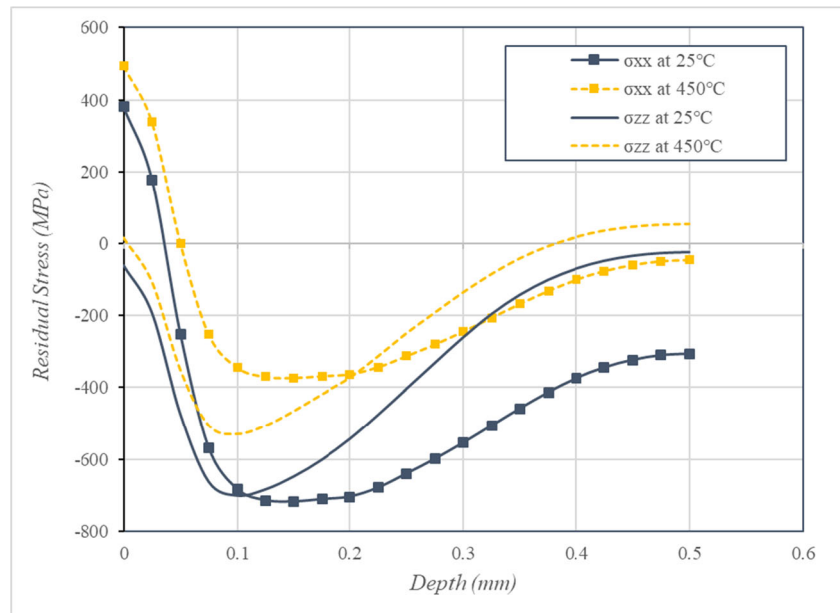

Fig. 9 Comparing tangential residual stress profile through the depth obtained using FE and experiment at room temperature

Fig. 10 Residual stress profiles in axial and tangential directions at 25 °C and 450 °C

the stresses. As it was discussed before, the anisotropy of the developed residual stresses at room temperature can be explained by the plastic deformations caused during the process.

3 Design of experiments and response surface method

Each simulation run of the DCR process and the following spring back and thermal relaxation analysis took about 188 h on a computer with four core i7 2.70 GHz CPU and 64 GB available RAM. As it can be realized, performing sensitivity analysis, design optimization, or assessing uncertainty of the process parameters on the residual stress profiles using FE simulation models is computationally expensive and impractical.

The development of an efficient methodology to establish an explicit correlation between process parameters and the residual stress profiles (at both room temperature and 450 °C) are discussed in this section. The depth of the created compressive layer and the distribution of dislocation density caused by cold working of the surface layers depend upon the process parameters such as ball size, rolling pressure, feed, and the rolling speed. The previous experimental and numerical research works have unanimously confirmed that the impact of the rolling speed on the residual stress is negligible [5, 16, 29, 30]. Therefore, ball diameter D (6–12 mm), the feed f (0.05–0.20 mm), and the fluid pressure P (10–30 MPa) are considered as design variables (design features) in the current study.

Design of experiments (DoE) has been employed to discretize the design domain at intelligently selected sampling points named design points. The design points are the most representative input configurations for simulation or physical experiments at a given design domain. DoE refers to a collection of statistical techniques that provide a framework to maximize the knowledge sought over a design domain with minimum number of required simulations (or experiments) performed at the design points [4, 31].

Ten output responses have been considered in the current study which can effectively describe the residual stress profile.

- The summation of the total area of the residual stress calculated using both negative and positive areas of the stress components throughout the thickness in x and z directions, i.e., [$Area\ \sigma_{xx} + Area\ \sigma_{zz}$] which represents the depth of the residual stress. This will be represented by $(Area)_{RT}$ and $(Area)_{450}$ for room temperature and 450 °C, respectively.

- The residual stress components (parallel and perpendicular to the rolling direction) on the surface of the workpiece which are represented by $(\sigma_{0xx})_{RT}$ and $(\sigma_{0zz})_{RT}$ at room temperature. $(\sigma_{0xx})_{450}$ and $(\sigma_{0zz})_{450}$ will be used to show the residual stresses at 450 °C.

- The residual stress components in the depth of 500 μm (mid thickness the workpiece) which are represented by $(\sigma_{500xx})_{RT}$ and $(\sigma_{500zz})_{RT}$ at room temperature. $(\sigma_{500xx})_{450}$ and $(\sigma_{500zz})_{450}$ will be used to show the residual stresses at 450 °C.

Central composite design (CCD) method available in Minitab© software was used to design the experiment and identify the design points [32]. The developed high-fidelity FE model has then been executed at each design point to evaluate the desired output responses described above. Tables 2 and 3 summarize the design points and their

Table 2   Design points and the FE results (training data set) at room temperature

D (mm)	f (mm)	P (MPa)	$(\sigma_{0xx})_{RT}$ (MPa)	$(\sigma_{0zz})_{RT}$ (MPa)	$(\sigma_{500xx})_{RT}$ (MPa)	$(\sigma_{500zz})_{RT}$ (MPa)	$(Area)_{RT}$ (MPa m)
6	0.050	10	− 44	− 80	156	575	− 0.4907
6	0.200	10	285	− 144	− 71	233	− 0.6530
6	0.050	30	314	244	− 822	56	− 1.1037
6	0.200	30	216	− 504	− 446	− 550	− 1.2341
6	0.125	20	153	54	− 651	− 326	− 1.1461
9	0.050	20	− 132	200	− 947	− 141	− 1.1846
9	0.200	20	110	− 257	− 522	− 706	− 1.2258
9	0.125	10	126	327	− 749	− 247	− 1.1546
9	0.125	30	− 210	162	− 822	− 782	− 1.4541
9	0.125	20	− 82	123	− 861	− 674	− 1.3957
12	0.050	10	− 118	115	− 947	1	− 1.0802
12	0.200	10	110	− 73	− 660	− 716	− 1.2613
12	0.050	30	− 594	44	− 1105	− 544	− 1.4769
12	0.200	30	− 402	− 169	− 536	− 688	− 1.2911
12	0.125	20	− 333	174	− 814	− 781	− 1.4047

associated desired responses at room and elevated temperature of 450 °C, respectively.

Response surface methodology (RSM) which is a well-stablished regression-based technique has been utilized to train and validate the best polynomial approximate to the responses of interest (residual stress profile in this study), by minimizing the error of the approximation. The error between the exact response y (from FE simulation) and its approximation $\widehat{y}$ is represented by ε.

$$y = \widehat{y}(x_1, x_2, \ldots\ldots, x_n) + \varepsilon \qquad (2)$$

The RSM-based approximate response can be written as [33]

$$\widehat{y} = \beta_0 + \sum_{i=1}^{n} \beta_i x_i + \sum_{i=1}^{n} \sum_{j=i+1}^{n} \beta_{ij} x_i x_j + \sum_{i=1}^{n} \beta_{ii} x_i^2 + \qquad (3)$$

where x_i are the design variables (design feature) and β_i are the polynomial coefficients to be calculated. Using the least square technique, an optimization problem is solved to minimize the square error of approximate response to known exact response over the entire training set. The surrogate models developed by RSM are smooth and quick to calculate, so they can be efficiently employed in any gradient-based and derivative-free optimization algorithms [31].

The accuracy of the developed surrogate models is usually examined by R^2 (i.e., R-squared) which is also known as the coefficient of determination. R^2 is a statistical measure of how

Table 3   Design points and the FE results (training data set) at 450 °C

D (mm)	f (mm)	P (MPa)	$(\sigma_{0xx})_{450}$ (MPa)	$(\sigma_{0zz})_{450}$ (MPa)	$(\sigma_{500xx})_{450}$ (MPa)	$(\sigma_{500zz})_{450}$ (MPa)	$(Area)_{450}$ (MPa m)
6	0.050	10	21	− 48	196	458	− 0.3180
6	0.200	10	328	− 79	69	226	− 0.3615
6	0.050	30	430	246	− 473	92	− 0.6403
6	0.200	30	266	− 203	− 267	− 259	− 0.7068
6	0.125	20	252	144	− 394	− 326	− 0.6946
9	0.050	20	100	249	− 582	− 49	− 0.6874
9	0.200	20	180	− 5	− 315	− 350	− 0.6669
9	0.125	10	235	353	− 468	− 114	− 0.7060
9	0.125	30	− 40	295	− 522	− 440	− 0.8531
9	0.125	20	64	240	− 575	− 408	− 0.8609
12	0.050	10	96	163	− 534	55	− 0.5959
12	0.200	10	193	142	− 422	− 377	− 0.7011
12	0.050	30	− 228	138	− 647	− 356	− 0.8542
12	0.200	30	− 156	106	− 282	− 347	− 0.6629
12	0.125	20	− 97	320	− 508	− 461	− 0.8090

close the data are to the fitted regression models and is always between 0 and 100% in which a model with a higher R^2 better fits the training data. The coefficient of determination, R^2, can be presented as:

$$R^2 = 1 - \frac{\sum_{i=1}^{n} \left(y_i - \widehat{y}_i\right)^2}{\sum_{i=1}^{n} \left(y_i - \overline{y}\right)^2} \tag{4}$$

where $\overline{y}$ is the mean of the observed data (here the FE results). It can be realized from Eq. (3) that several types of polynomial such as the linear, quadratic, and cubic functions can be considered for the surrogate models. In this research study, a quadratic model was considered for the response surface functions as R^2 value over 85% can be achieved without overfitting the training data set by higher-order polynomials. The reduced quadratic response surface functions for the desired output responses are presented in Eqs. (5) to (14) and the R^2 values of each developed surrogate model is presented beside it in a bracket which shows the high accuracy of the models to approximate the responses of interest.

$$(\sigma_{0xx})_{RT} = -362 + 31.0*D + 793*f + 47.22*P \tag{5}$$
$$+ 7764*f^2 - 5.322*D*P - 77.2*f*P, \left(R^2 = 95.88\%\right)$$

$$(\sigma_{0zz})_{RT} = -780 + 113*D + 7173*f$$
$$+ 11.17*P - 6.94*D^2 - 36425*f^2$$
$$+ 230*D*f - 118.4*f*P, \left(R^2 = 87.63\%\right) \tag{6}$$

$$(\sigma_{500xx})_{RT} = 3316 - 470*D - 9733*f - 108.6*P$$
$$+ 13.1*D^2 + 20617*f^2 + 0.651*P^2$$
$$+ 392*D*P + 5.5*D*P$$
$$+ 147.7*f*P, \left(R^2 = 93.31\%\right) \tag{7}$$

$$(\sigma_{500zz})_{RT} = 2976 - 155.9*D - 14294*f - 116.6*P$$
$$+ 44511*f^2 + 1.591*P^2$$
$$+ 3.27*D*P, \left(R^2 = 94.48\%\right) \tag{8}$$

$$(Area)_{RT} = 1.774 - 0.3278*D - 9.36*f - 0.0563*P$$
$$+ 0.0116*D^2 + 30.34*f^2 + 0.003198*D*P$$
$$+ 0.0664*f*P, \left(R^2 = 95.46\%\right) \tag{9}$$

$$(\sigma_{0xx})_{450} = -396 + 67.4*D + 96*f$$
$$+ 42.63*P - 1.77*D^2$$
$$+ 8339*f^2 \tag{10}$$
$$- 4.255*D*P - 82.8*f*P, \left(R^2 = 91.25\%\right)$$

$$(\sigma_{0zz})_{450} = -974 + 146.6*D + 5925*f$$
$$+ 18.24*P - 7.24*D^2 - 31135*f^2$$
$$+ 245*D*f - 1.029*D*P - 68.9*f*P, \left(R^2 = 89.88\%\right) \tag{11}$$

$$(\sigma_{500xx})_{450} = 2212 - 95.1*D - 12035*f - 91.7*P$$
$$+ 36874*f^2 + 1.295*P^2 + 1.96*D*P$$
$$+ 53.7*f*P, \left(R^2 = 93.61\%\right) \tag{12}$$

$$(\sigma_{500zz})_{450} = 2647 - 400*D - 8200*f - 61.2*P$$
$$+ 13.09*D^2 + 21402*f^2 + 222*D*f$$
$$+ 4.30*D*P$$
$$+ 97.6*f*P, \left(R^2 = 93.19\%\right) \tag{13}$$

$$(Area)_{450} = -1.086 - 0.1966*D - 7.108*f - 0.03282*P$$
$$+ 0.00718*D^2 + 24.76*f^2$$
$$+ 0.00186*D*P$$
$$+ 0.0458*f*P, \left(R^2 = 92.20\%\right) \tag{14}$$

4 Response surface of residual stress profiles

Figures 11 (a) and (b) show, respectively, the response surfaces of $(\sigma_{0xx})_{RT}$ and $(\sigma_{oxx})_{450}$ with respect to ball diameter and rolling pressure for the given feed of $f = 0.125$ mm. As it can be seen for the given feed, increasing the rolling pressure at smaller ball diameter increases $(\sigma_{0xx})_{RT}$ toward tensile region while at larger ball diameter decreases more toward the compressive region. Therefore, the impact of the rolling pressure on the axial residual stress highly depends on ball diameter. The similar trend can also be observed for $(\sigma_{oxx})_{450}$ in which increasing the rolling pressure increases $(\sigma_{oxx})_{450}$ toward the tensile region for the smaller ball diameter while decreases $(\sigma_{oxx})_{450}$ toward compressive region for the larger ball diameters. Comparing the surface plot of $(\sigma_{oxx})_{450}$ with its counterpart at room temperature shows that the thermal relaxation significantly reduces the magnitude of the compressive axial residual stress on the surface and the level of relaxation is significantly higher at the upper bound of the parameters where the plastic deformation is higher.

Figures 12 (a) and (b) also show the surface plot of $(\sigma_{0zz})_{RT}$ and $(\sigma_{0zz})_{450}$ with respect to ball diameter and feed for the given rolling pressure of 20 MPa, respectively. Results clearly show the dominant effect of feed on the responses. For $(\sigma_{0zz})_{RT}$, a higher value of feed is required to guarantee a compressive surface residual stress in tangential direction. It can be concluded from the results that the desirable compressive
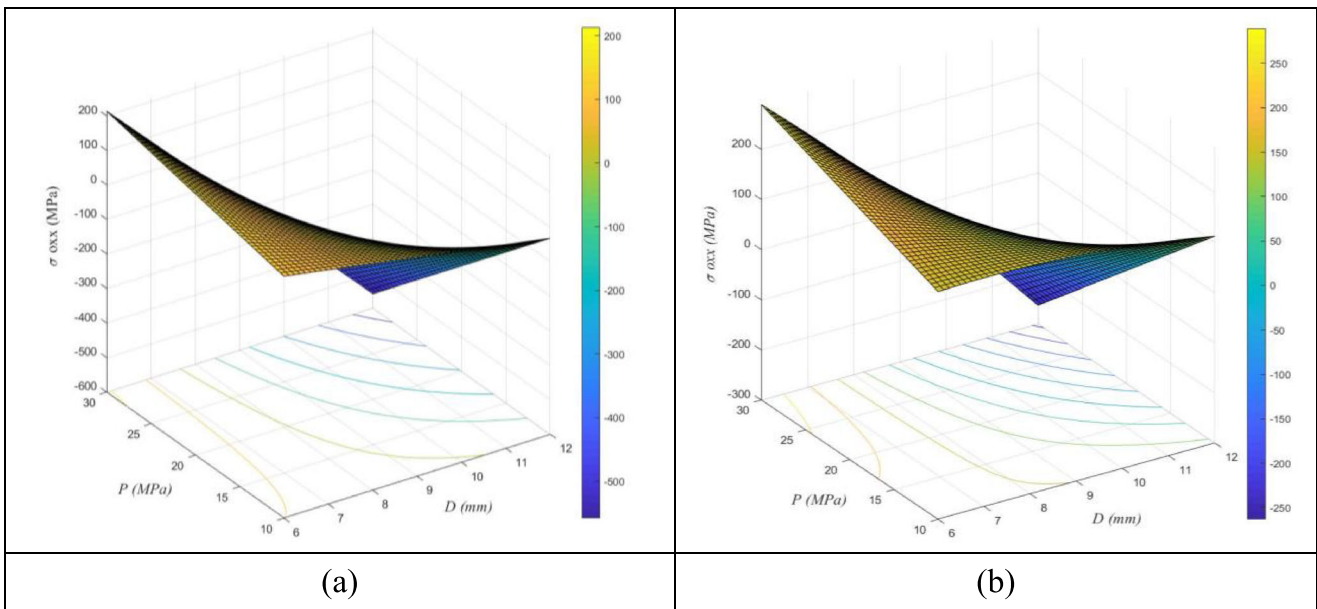
Fig. 11 Effect of ball diameter and rolling pressure on σ_{0xx} for f = 0.125 mm **a** at room temperature 25 °C and **b** at elevated temperature 450 °C

residual stress for $(\sigma_{0zz})_{RT}$ is only achievable at higher feed values. As it can be realized, results show a parabolic relation between the introduced tangential residual stresses and the feed. It is noted that similar parabolic behavior has been previously reported for conventional deep rolling of Ti-6Al-4V [4, 34] and AISI1045 [35]. With respect to $(\sigma_{0zz})_{450}$, one can realize that a high level of feed is required to maintain a compressive residual stress in tangential direction, particularly for small ball diameters. Moreover, comparing Figs. 12 (a) and (b) shows that thermal relaxation decreases the magnitude of the compressive tangential residual stress on the surface at a higher rate compared with tensile tangential residual stresses.

This is mainly attributed to thermal softening and net material movement of the surrounding material (untreated regions) and therefore imposing a less restrain on the treated region with compressive residual stress.

The results presented in Figs. 11 and 12 show that the thermal relaxation of residual stresses on surface is higher when they are induced by higher rolling pressure and feeds (upper bounds of the design variables). This agrees with the experimental findings [10, 34], where surface layers with medium dislocation density show a better thermal stability of residual stresses compared with surface layers with extremely high dislocation densities. Nevertheless, it can be realized that the residual stress can alter
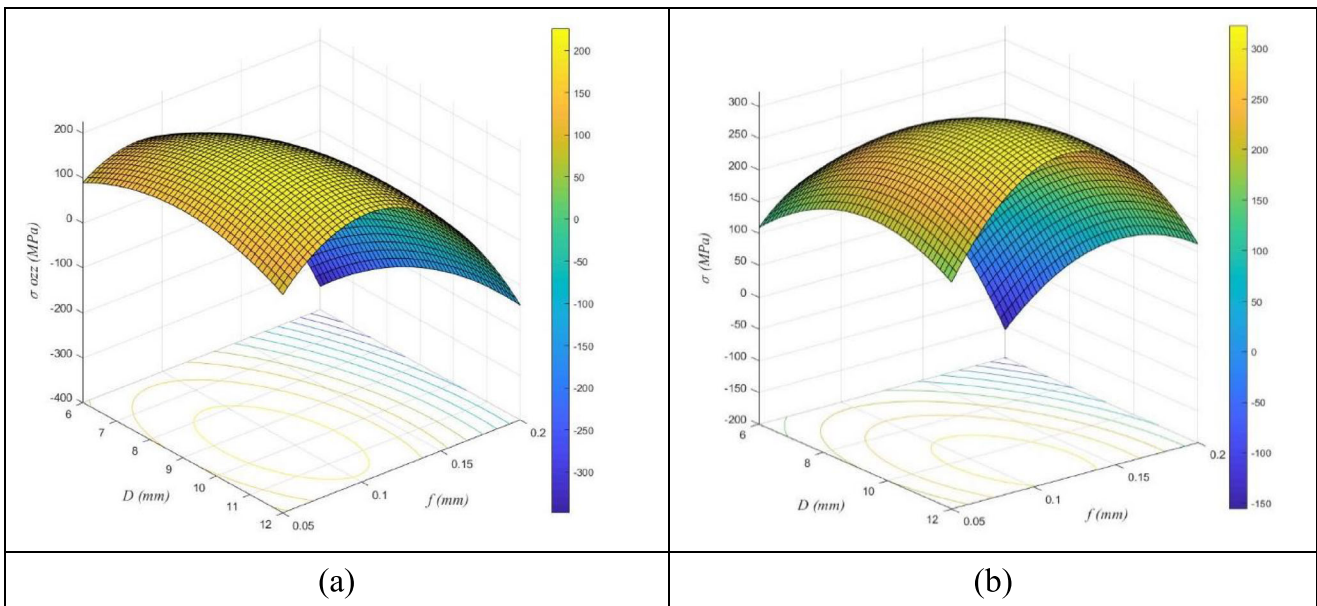

Fig. 12 Effect of feed and ball diameter on σ_{0zz} for P = 20 MPa **a** at room temperature 25 °C and **b** at elevated temperature 450 °C
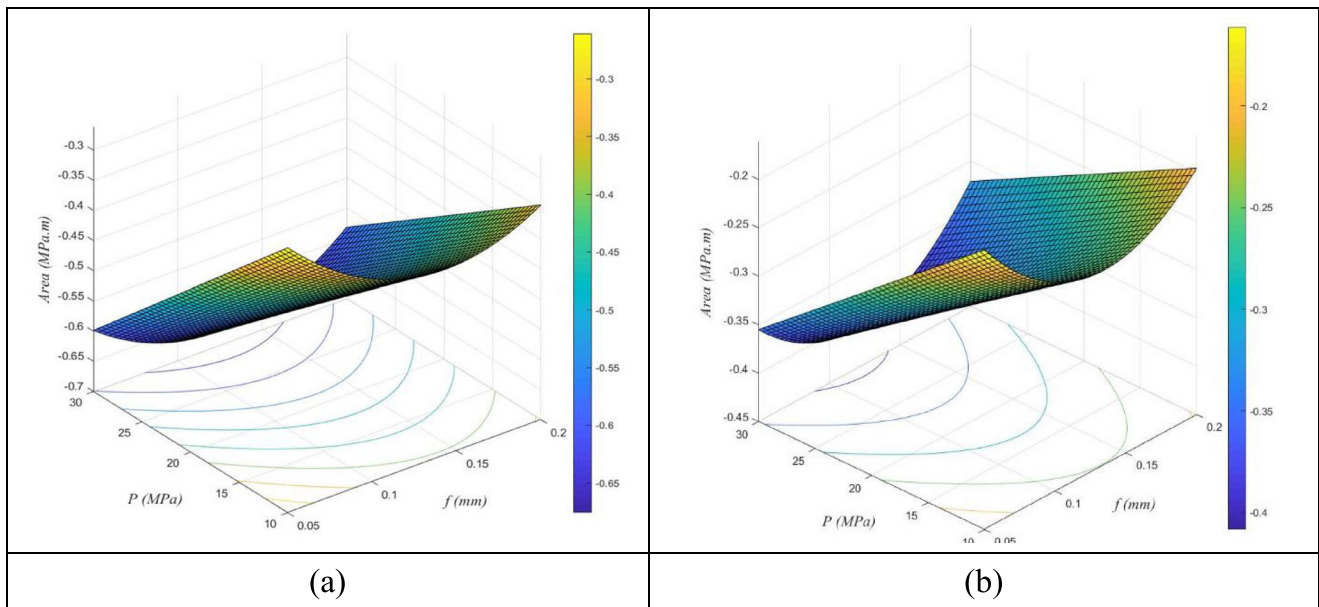
Fig. 13 Effect of feed and ball diameter on the stress *Area* for *D* = 6 mm **a** at room temperature 25 °C and **b** at elevated temperature 450 °C

from compressive to tensile at lower feed as the plastic deformation in tangential direction is not high enough to maintain a compressive residual stress at elevated temperature.

The response surfaces for $(Area)_{RT}$ and $(Area)_{450}$ with respect to rolling pressure and feed for the given ball diameter of 6 mm are presented in Fig. 13 (a) and (b), respectively. As it can be realized, both $(Area)_{RT}$ and $(Area)_{450}$ are more dominated by the rolling pressure and for the assumed ball diameter, increasing the rolling pressure creates a deeper residual stress profile at any given feed. However, comparing Fig. 13 (a) and (b), one can conclude that the exposure to the elevated temperature leads to decreasing the depth of the residual stress

profiles induced at the room temperature. It is noted that feed has more significant effect on the residual stress closer to the surface layer while the profile of the residual stresses through the depth of the component is more affected by the rolling pressure. The stress relaxation is basically more dependent on the level of rolling pressure than the feed and the residual stress profile relaxes more when the process is performed under higher rolling pressure.

Figures 14 and 15 respectively show the surface plots of (σ_{500xx}) and (σ_{500zz}), with respect to ball diameters and rolling pressure for feed f = 0.125 mm at both room and 450 °C temperatures. The output responses show a very similar behavior
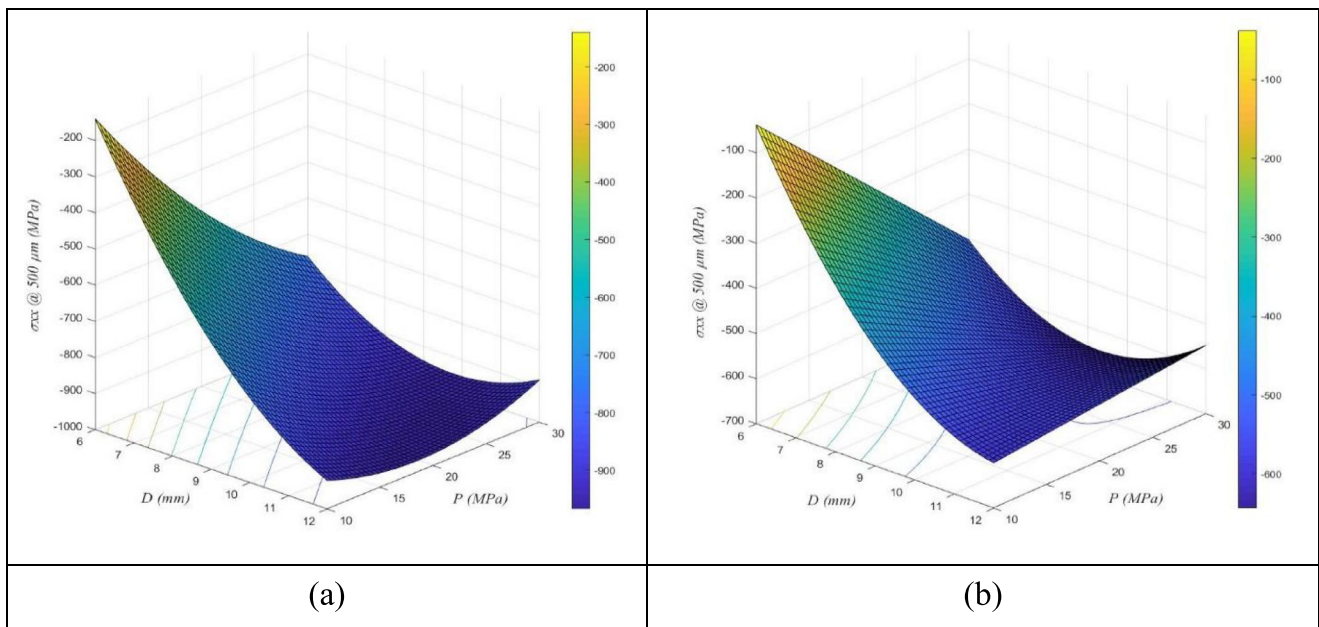

Fig. 14 Effect of rolling pressure and ball diameter on σ_{500xx} for f = 0.125 mm **a** at room temperature 25 °C and **b** at elevated temperature 450 °C

Fig. 15 Effect of rolling pressure and ball diameter on σ_{500zz} for $f = 0.125$ mm **a** at room temperature 25 °C and **b** at elevated temperature 450 °C
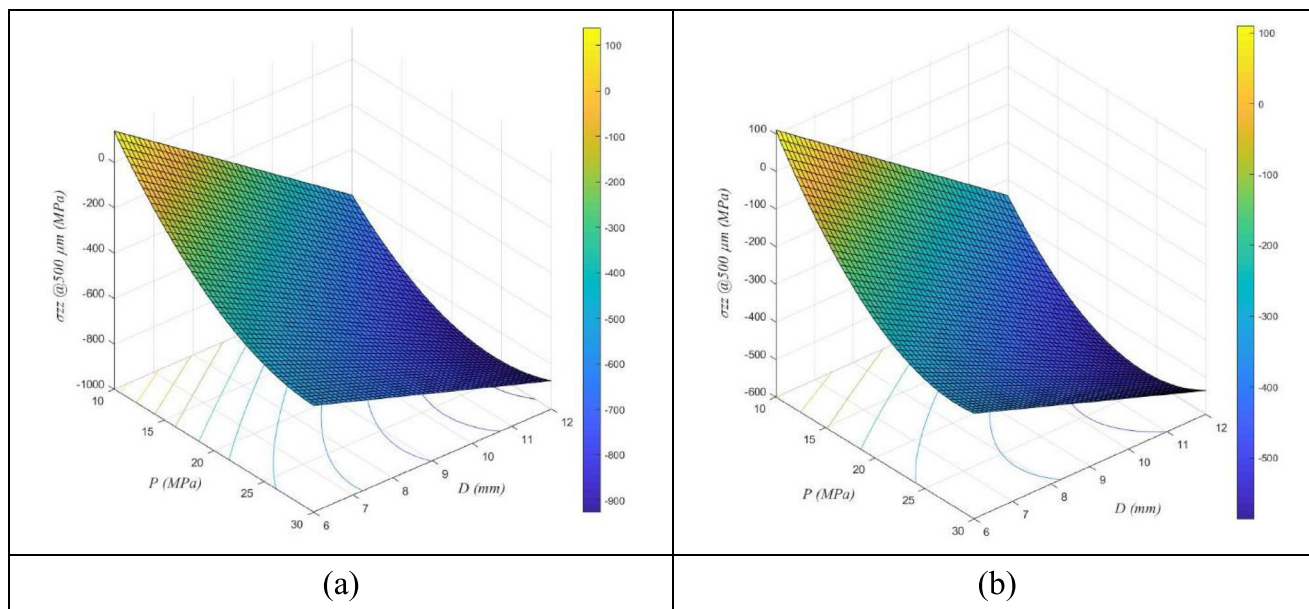
with respect to the design variables. As it can be realized, the effect of the rolling pressure is more significant at smaller ball diameter where increasing the rolling pressure leads to a more compressive residual stress. However, at higher ball diameters, a parabolic behavior is observed which may be attributed to deep strain hardening introduced due to process applied from both sides which interact around mid-surface of the component. The thermal relaxation especially at higher ball diameter is mainly dominated by material softening as the plastic strains are developed through the entire thickness.

5 Optimization

As it was explained and shown in the previous sections, the double-sided DCR process induces anisotropic residual stress profiles which are significantly different in axial and tangential directions. Therefore, the process parameters need to be tailored according to the stresses imposed by the external loading. The double-sided deep rolling of a compressor blade of a gas turbine which is schematically presented in Fig. 16 has been considered in the current study for the optimization problem. The external loads on the blades are centrifugal force (CF) due to the shaft rotation and pressure load imposed by

the hot gas. These loads result in significant radial stress in Z' direction and moments around X' axis ($M_{X'}$) at the inner platform zone highlighted in blue. The aerodynamic definition of the airfoil also results in a very thin trailing edge (zone highlighted in red) which results in high radial stress in this region. Therefore, the surface treatment can be efficiently employed to enhance the fatigue life of the component by introducing a compressive residual stress in the highlighted zones without any design change.

The application of the double-sided DCR process in the highlighted zones of the blade is constrained by the rolling direction imposed by the geometry. As it can be realized, the double-sided DCR in blue and red zones can be practically performed only in global X' and Z' directions, respectively. Therefore, while the objective in the blue zone is to achieve the most compressive residual stress perpendicular to the rolling direction (σ_{0zz}) (note that rolling direction, x in blue region, coincides with global X'), the objective in the red zone is to achieve the most compressive stress in the rolling direction (σ_{0xx}), (note that rolling direction, x in red region, coincides with global Z').

The proposed multi-objective design optimization problem can be formally formulated as:

$$\begin{aligned}
\text{minimize the function} \quad & 0.5 \; \overline{Area + w_1(\sigma_0)_{zz} + w_2(\sigma_0)_{xx}} \\
\text{Subject to the constarint} \quad & w_1(\sigma_{500})_{zz} + w_2(\sigma_{500})_{xx} < -100 MPa \\
& 6 \; mm \leq D \leq 12 \; mm \\
& 0.05 \; mm \leq f \leq 0.2 \; mm \\
& 10 \; MPa \leq P \leq 30 \; MPa
\end{aligned} \tag{15}$$

The defined constraint function will guarantee that a sufficient compressive residual stress is introduced throughout the thickness while avoiding a tensile balancing stress at the mid-thickness of the workpiece. The proposed objective function can be tailored based on the stress distribution in the blade due to the external applied load using the weighting factors provided in Table 4.

The developed analytical response functions given in Eqs. (5)–(14) are effectively used to establish the objective and constraint functions formulated in Eq. (15) with respect to the design variables at both 25 °C and 450 °C operating temperatures. Considering this, the optimization problem formulated in Eq. (15) can be efficiently solved using gradient-based optimization algorithms.

A combination of sequential quadratic programming (SQP) and genetic algorithm (GA) techniques is employed in the current study to solve the optimization problem. SQP is a local optimizer without any mechanism to search for global solution but it is a powerful non-linear mathematical programming technique which can capture a local optimum solution accurately. On the other hand, genetic algorithm (GA) is a widely used and popular stochastic-based global optimizer. In this
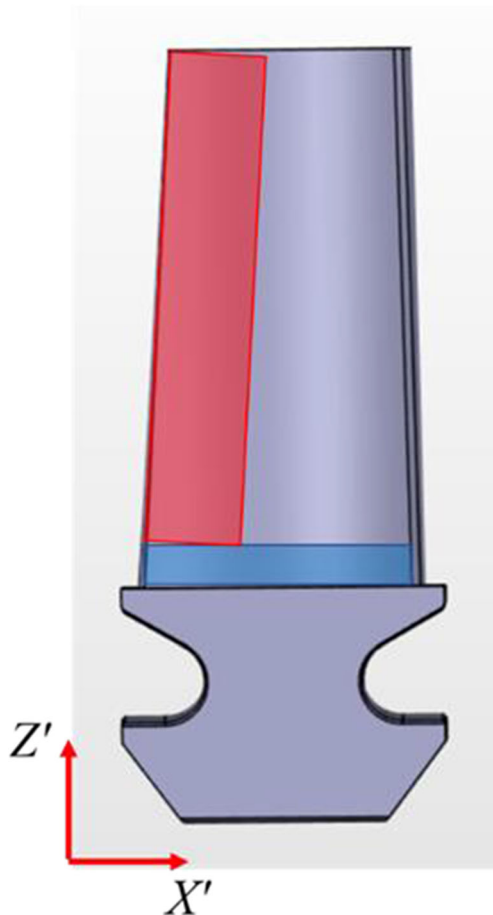
hybrid method, the optimal solutions from GA which are in neighborhood of the true optimum solution are forwarded as the initial points to the SQP solver in order to accurately capture the global optimal solutions. This method has been successfully employed in design optimization of multiphysics problems where finding a global solution was not analytically guaranteed [31].

6 Results and discussions

Design optimization problem formulated in the previous section has been used to obtain the optimum set of design variables (i.e., ball diameter, rolling pressure, and rolling feed) in order to achieve an optimal residual stress profile at room and after relaxation at elevated temperature of 450 °C. The optimization problems were solved using the proposed GA combined with SQP method.

Tables 5 and 6 present the process parameters to achieve optimal residual stress profiles at the identified critical areas at 25 °C and 450 °C, respectively. As it can be realized from comparing Tables 5 and 6, the operating temperature slightly changes the optimal design variables for surface treatment of the trailing edge. For further clarification, the desired output responses at 450 °C have been evaluated using the optimal design process parameters (optimal D, f, and P) obtained at room temperature and compared with those optimal values obtained at 450 °C and the results are provided in Table 7. The optimal results obtained for double-sided DCR is less sensitive to the operating temperature compared with those

Table 4 Assigned weighting factors in the optimization problem

Treated area	w_1	w_2
Inner platform zone (blue zone)	0.5	0
Trailing edge zone (red zone)	0	0.5

Fig. 16 Schematic of a compressor blade and the treated areas

Table 5 Optimization results at 25 °C

	Inner platform zone	Trailing edge zone
w_1	0.5	0
w_2	0	0.5
D (mm)	6.00	12.00
f (mm)	0.200	0.112
P (MPa)	30.00	30.00
$(\sigma_{0xx})_{RT}$ (MPa)	289	− 563
$(\sigma_{0zz})_{RT}$ (MPa)	− 474	170
$(Area)_{RT}$ (MPa m)	− 1.1644	− 1.5347
$(\sigma_{500xx})_{RT}$ (MPa)	− 515	− 825
$(\sigma_{500zz})_{RT}$ (MPa)	− 480	− 940

Table 6 Optimization results at 450 °C

	Inner platform zone	Trailing edge zone
w_1	0.5	0
w_2	0	0.5
D (mm)	6.00	12.00
f (mm)	0.200	0.129
P (MPa)	30	30
$(\sigma_{0xx})_{450}$ (MPa)	314	− 264
$(\sigma_{0zz})_{450}$ (MPa)	− 173	279
$(Area)_{450}$ (MPa m)	− 0.6413	− 0.8823
$(\sigma_{500xx})_{450}$ (MPa)	− 201	− 540
$(\sigma_{500zz})_{450}$ (MPa)	− 276	− 538

obtained for conventional DCR. This is mainly attributed to the more uniform residual stress distribution through the thickness induced by the double-sided process as presented in Fig. 4.

7 Conclusion

A high-fidelity finite element (FE) model has been developed to predict the axial and tangential residual stress profiles induced by double-sided DCR process on Ti64 thin plate at the room temperature and the following thermal relaxation at elevated temperature. The results obtained from the developed FE model are in good agreement with available experimental measurements.

The developed FE model was then utilized to generate training data at intelligently identified design points using DoE techniques. Response surface methodology was subsequently employed to train and validate predictive analytical models. The developed surrogate analytical models can efficiently replace full-scale and computationally expensive FE simulation and accurately predict the residual stress profiles at room temperature and after thermal relaxation at 450 °C.

Table 7 Output results at 450 °C using optimal design variables obtained at room temperature versus at elevated temperature for the trailing edge zone

	Optimized at 25 °C	Optimized at 450 °C
D (mm)	12.00	12.00
f (mm)	0.112	0.129
P (MPa)	30.00	30.00
$(\sigma_{0xx})_{450}$ (MPa)	− 258	− 264
$(\sigma_{0zz})_{450}$ (MPa)	290	279
$(Area)_{450}$ (MPa m)	− 0.8858	− 0.8823
$(\sigma_{500xx})_{450}$ (MPa)	− 513	− 540
$(\sigma_{500zz})_{450}$ (MPa)	− 580	− 538

The effects of ball dimeter, feed and rolling pressure on the induced residual stress profiles, and their thermal relaxations at elevated temperature were systematically investigated using the developed surrogate models. A design optimization problem was formulated to enhance fatigue life at high stress locations of a generic compressor blade considering different operating temperatures. The developed analytical surrogate models were used to describe the objective and constraint functions. The conclusions and highlights of the present study are outlined as follows:

1. The residual stress profile induced by double-sided DCR process is significantly different than that induced by the conventional DCR process performed on the same workpiece under identical processing parameters.
2. The process generates residual stress profiles which are anisotropic and significantly different in axial and tangential directions. Therefore, the stress distribution in the component due to external load should be known prior to selection of the rolling direction.
3. Higher rolling pressure and larger ball diameters with lower feed are required to achieve a more compressive residual stress in the axial direction $(\sigma_{oxx})_{RT}$. The tangential residual stress is mainly affected by feed as it significantly influences the tangential plastic deformation and higher feed values are required to achieve more compressive residual stress in tangential direction.
4. At any given ball diameter, the level of thermal relaxation is higher for deeper and more compressive residual stress which is due to high plastic deformation and thermal instability of dislocations. While the rate of thermal relaxation of axial residual stress is more pronounced at lower feed and higher pressure, the tangential residual stress relaxes more when the process is conducted under higher levels of pressure and feed.
5. The operating temperature of the components and the stress imposed by external loading need to be considered in the optimization problem.

References

1. Tsuji N, Tanaka S, Takasugi T (2008) Evaluation of surface-modified Ti–6Al–4V alloy by combination of plasma-carburizing and deep-rolling. Mater Sci Eng A 488(1):139–145
2. Nalla RK, Altenberger I, Noster U, Liu GY, Scholtes B, Ritchie RO (2003) On the influence of mechanical surface treatments-deep rolling and laser shock peening-on the fatigue behavior of Ti-6Al-4V at ambient and elevated temperatures. Mater Sci Eng A 355(1-2):216–230
3. Bäcker V, Klocke F, Wegner H, Timmer A, Grzhibovskis R, Rjasanow S (2010) Analysis of the deep rolling process on turbine blades using the FEM/BEM-coupling. IOP Conf Ser Mater Sci Eng 10(1):012134

4. Hadadian A, Sedaghati R (2019) Investigation on thermal relaxation of residual stresses induced in deep cold rolling of Ti–6Al–4V alloy. Int J Adv Manuf Technol 100(1-4):877–893

5. Klocke F, Bäcker V, Wegner H, Feldhaus B, Baron HU, Hessert R (2009) Influence of process and geometry parameters on the surface layer state after roller burnishing of IN718. Prod Eng 3(4-5):391–399

6. Prevéy PS, Ravindranath RA, Shepard M et al. (2003) Case studies of fatigue life improvement using low plasticity burnishing in gas turbine engine applications. In: ASME Turbo Expo 2003, collocated with the 2003 International Joint Power Generation Conference. American Society of Mechanical Engineers, p 657

7. Gill C, Fox N, Withers P (2008) Shakedown of deep cold rolling residual stresses in titanium alloys. J Phys D 41(17):174005

8. Altenberger I, Nalla R, Noster U et al. (2002) On the fatigue behavior and associated effect of residual stresses in deep-rolled and laser shock peened Ti-6Al-4V alloys at ambient and elevated temperatures. University of California, Berkeley 94720

9. Prevey P, Hornbach D, Ravindranath R et al. (2003) Application of low plasticity burnishing to improve damage tolerance of a Ti-6Al-4V first stage fan blades. In: 44th AIAA/ASME/ASCE/AHS/ASC Structures, Structural Dynamics, and Materials Conference, p 1524

10. Prevéy P, Hombach D, Mason P (1998) Thermal residual stress relaxation and distortion in surface enhanced gas turbine engine components. In: Milam DL (ed) Proceedings of the 17th Heat Treating Society Conference, Indianapolis, IN, Sept 15–18, 1997. ASM

11. El-Axir M (2000) An investigation into roller burnishing. Int J Mach Tools Manuf 40(11):1603–1617

12. Loh N, Tam S, Miyazawa S (1989) A study of the effects of ball-burnishing parameters on surface roughness using factorial design. J Mech Work Technol 18(1):53–61

13. Prabhu P, Kulkarni S, Sharma S (2010) Influence of deep cold rolling and low plasticity burnishing on surface hardness and surface roughness of AISI 4140 steel. World Acad Sci Eng Technol 72:619–624

14. Seemikeri C, Brahmankar P, Mahagaonkar S (2008) Investigations on surface integrity of AISI 1045 using LPB tool. Tribol Int 41(8):724–734

15. Scheil J, Müller C, Steitz M et al (2013) Influence of process parameters on surface hardening in hammer peening and deep rolling. Key Eng Mater 554:1819–1827

16. Mohammadi F, Sedaghati R, Bonakdar A (2013) Finite element analysis and design optimization of low plasticity burnishing process. Int J Adv Manuf Technol 70(5-8):1337–1354

17. Klocke F, Bäcker V, Timmer A et al (2009) Innovative FE-analysis of the roller burnishing process for different geometries. In: X international conference on computational plasticity fundamentals and application. Barcelona, Spain, p 1

18. Sayahi M, Sghaier S, Belhadjsalah H (2013) Finite element analysis of ball burnishing process: comparisons between numerical results and experiments. Int J Adv Manuf Technol 67(5-8):1665–1673

19. Lim A, Castagne S, Wong CC (2016) Effect of deep cold rolling on residual stress distributions between the treated and untreated regions on Ti–6Al–4V alloy. J Manuf Sci Eng 138(11):111005

20. Klocke F, Bäcker V, Wegner H, Zimmermann M (2011) Finite element analysis of the roller burnishing process for fatigue resistance increase of engine component. Proceedings of the Institution of Mechanical Engineers, P I Mech Eng B-J Eng 225(1):2–11

21. Klocke F, Mader S (2005) Fundamentals of the deep rolling of compressor blades for turbo aircraft engines. Steel Res Int 76(2-3):229–235

22. Anonymous (2006) Tools & solutions for metal surface improvement, roller burnishing, deep rolling, combined skive-burnishing. In: ECOROLL© Corporation Tool Technology. ECOROLL© Corporation Tool Technology. Available via . http://www.utech.co.th/files/ecoroll_catalog_en_web.pdf 2019

23. Kıranlı E (2009) Determination of material constitutive equation of a biomedical grade Ti6AI4V alloy for cross-wedge rolling. Master of Science in Material Science, Izmir Institute of Technology

24. Sun J, Guo Y (2009) Material flow stress and failure in multiscale machining titanium alloy Ti-6Al-4V. Int J Adv Manuf Technol 41(7):651–659

25. Lesuer DR (2000) Experimental investigation of material models for Ti-6Al-4V and 2024-T3. FAA Report DOT/FAA/AR-00/25

26. Lee W, Lin C (1998) Plastic deformation and fracture behaviour of Ti–6Al–4V alloy loaded with high strain rate under various temperatures. Mater Sci Eng A 241(1):48–59

27. Haight S, Wang L, Du Bois P et al. (2016) Development of a titanium alloy Ti-6Al-4V material model used in LS-DYNA DOT/FAA/TC-15/23

28. Stanojevic A, Maderbacher H, Angerer P et al. (2016) Stability of residual stresses in Ti-6Al-4V components due to mechanical loads. In: Venkatesh V (ed) Proceedings of the 13th World Conference on Titanium. Wiley Online Library, Hoboken, NJ, USA., p 1593

29. Majzoobi G, Jouneghani FZ, Khademi E (2016) Experimental and numerical studies on the effect of deep rolling on bending fretting fatigue resistance of Al7075. Int J Adv Manuf Technol 82(9-12):2137–2148

30. Yen Y (2004) Modeling of metal cutting and ball burnishing - prediction of tool wear and surface properties, The Ohio State University

31. Hadadian A, Sedaghati R, Esmailzadeh E (2013) Design optimization of magnetorheological fluid valves using response surface method. J Intell Mater Syst Struct 25(11):1352–1371

32. Minitab 18 Statistical Software (2018) [Computer software]. Minitab, Inc. (www.minitab.com). Minitab 18 Support. Available via . https://support.minitab.com/en-us/minitab/18/?SID=0;. Accessed 1/1 2019

33. Hadadian A (2011) Optimal design of magnetorheological dampers constrained in a specific volume using response surface method, Concordia University

34. Prevéy PS, Shepard MJ, Smith PR (2001) The effect of low plasticity burnishing (LPB) on the HCF performance and FOD resistance of Ti-6AI-4V. In: The 6th National Turbine Engine High Cycle Fatigue (HCF) Conference, 5–8 March 2001(Jacksonville, Florida, USA). DTIC Document

35. Loh N, Tam S, Miyazawa S (1989) Statistical analyses of the effects of ball burnishing parameters on surface hardness. Wear 129(2):235–243